Materials and Design 198 (2021) 109368

Contents lists available at ScienceDirect

Materials and Design

journal homepage: www.elsevier.com/locate/matdes

Thermoplastic forming of additively manufactured Zr-based bulk metallic glass: A processing route for surface finishing of complex structures

Maximilian Frey [a,*], Jan Wegner [b], Nico Neuber [a], Benedikt Reiplinger [a], Benedikt Bochtler [a,c], Bastian Adam [a], Lucas Ruschel [a], Sascha Sebastian Riegler [a], Hao-Ran Jiang [a,d], Stefan Kleszczynski [b], Gerd Witt [b], Ralf Busch [a]

[a] Chair of Metallic Materials, Saarland University, Campus C6.3, 66123 Saarbrücken, Germany
[b] Chair of Manufacturing Technology, University Duisburg-Essen, Lotharstraße 1, 47057 Duisburg, Germany
[c] Amorphous Metal Solutions GmbH, Michelinstraße 9, 66424 Homburg, Germany
[d] School of Materials Science and Engineering, Tongji University, 4800 Caoan Road, 201804 Shanghai, China

HIGHLIGHTS

- LPBF-formed AMZ4 metallic glass provides enough thermal stability for thermoplastic forming without harsh crystallization.
- With adequate process parameters, thermoplastic forming has no influence on the mechanical properties of LPBF-formed AMZ4.
- Thermoplastic forming allows to massively reduce the surface roughness of additively formed metallic glass specimen.
- Finely structured surface pattern can be imprinted on additively formed metallic glass parts via thermoplastic forming.

GRAPHICAL ABSTRACT

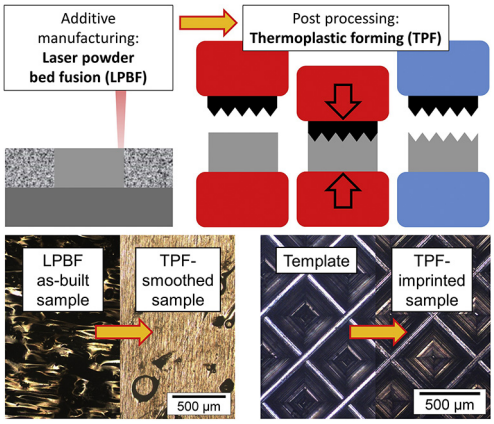

ARTICLE INFO

Article history:
Received 28 September 2020
Received in revised form 11 November 2020
Accepted 29 November 2020
Available online 30 November 2020

Keywords:
Bulk metallic glasses
Additive manufacturing
Laser powder bed fusion
Post-processing
Thermoplastic forming
Mechanical properties

ABSTRACT

Additive manufacturing of bulk metallic glasses (BMGs) through laser powder bed fusion (LPBF) has drawn growing interest in the last years, especially concerning industry-relevant alloys based on iron or zirconium. The process-inherent high cooling rates and localized melting pools allow to overcome geometrical restrictions given for the production of BMGs by classical casting routes. Yet, the achievable surface qualities are still limited, making an adequate post-processing necessary. In this work, we report on applying thermoplastic forming on LPBF-formed parts for the first time to decrease surface roughness and imprint finely structured surface patterns without the need for complex abrasive machining. This BMG-specific post-processing approach allows to functionalize surface areas on highly complex LPBF-formed specimens, which could be of interest especially for medical or jewelry applications.

* Corresponding author.
E-mail address: maximilian.frey@uni-saarland.de (M. Frey).

https://doi.org/10.1016/j.matdes.2020.109368

1. Introduction

Bulk metallic glasses (BMGs) are a relatively new class of engineering materials. Their combination of high strength and hardness on the one hand and elastic limits up to 2% similar to polymers on the other hand offers significant advantages over crystalline metals [1]. BMGs are produced by rapid cooling from the equilibrium liquid state to avoid crystallization until vitrification occurs at the glass transition temperature. Massive alloy development efforts resulted in various multicomponent alloys with high glass forming ability (GFA). A parameter that directly defines the GFA of a given system is the critical cooling rate (CCR), which is the slowest rate that ensures glass formation without crystallization effects during undercooling. BMGs are mostly produced via classical casting routes, where the high-temperature melt is poured, injected, or sucked into a (water-cooled) metallic mold. As the glassy specimen is monolithically produced by dissipating the heat of the liquid through the mold interface, the achievable cooling rates in the inner volume of a cast part decrease with sample thickness. This results in an upper size boundary for fully amorphous cast specimen that can be quantified by the critical casting thickness, which is the maximum diameter in which an amorphous rod-shaped sample can be cast. This size limitation, in combination with the typical geometric limitations of a casting process, hinders the industrial applicability of this material class until today. A novel approach to overcome these restrictions is the additive manufacturing of metallic glasses by laser powder bed fusion (LPBF) [2–5]. The layer-wise manufacturing approach with very small and localized melt pools, features high cooling rates up to 10^6 K/s [6]. This allows to create large and complexly shaped parts that cannot be produced by casting. Besides this advantage of LPBF-produced BMGs over cast specimens, the powder based process also inheres some drawbacks. The achievable surface quality is limited due to the powder feedstock material, staircase effects resulting from the layer-wise built-up, and sintered particles at the interface between the powder bed and the part. The resulting surface roughness limits the spectrum of possible applications, especially in the biomedical sector, where precisely defined surfaces are often needed [7]. Therefore, functional surfaces of LPBF-manufactured parts generally have to be post-processed to meet the requirements. In this context, several techniques such as electro-polishing [8] or abrasive flow machining [9] are subjects to current research. However, the achievable finish quality is often limited and can be detrimental for certain surface topographies such as open cavities and edges. Therefore, the development of adequate post-processing routes for complex surface structures is in high demand.

An interesting advantage of BMGs over common crystalline metals is the possibility of thermoplastic forming (TPF). Thereby, an initially glassy specimen is heated into the supercooled liquid state, where the viscosity ranges between roughly 10^{12} to 10^5 Pa s [10]. These conditions allow viscoplastic deformation through applied mechanical loads in analogy to thermoforming or blow molding processes known from thermoplastics or silicate glasses. The specimen can be formed into a desired geometry, followed by quick cooling into the glassy state to prevent undesired crystallization. High surface qualities are possible since even structures on the nanoscopic scale can be imprinted [11,12]. Recent studies about viscoplastic deformation of a LPBF-formed BMG have sparked interest to functionalize TPF post-processing for additive manufacturing [13]. Thus, the aim of this study is to demonstrate the possibility of combining both processes to synergize the geometrical freedom given by LPBF with the high-quality surface post-processing achievable by TPF.

2. Materials and methods

Gas-atomized powder of the commercially available glass forming alloy AMZ4 [14] (composition in at.%: $Zr_{59.4}Cu_{28.8}Al_{10.4}Nb_{1.5}$) with an oxygen content of about 1580 μg/g and a mean particle diameter x_{50} of 37.8 μm was provided by Heraeus Amloy Technologies GmbH. Beam-shaped samples ($1.9 \times 2.8 \times 25.2$ mm^3) and cylindrical specimen (12 mm diameter, 3 mm height) were produced under argon gas atmosphere using an eos M100 LPBF device that features a fiber laser with a wavelength of 1064 nm. The process parameters were set according to two previous studies by Wegner et al. to reach a volume energy density of 25 J/mm^3 and allow to produce samples with optical relative densities in the order of 99.5% or above [15,16].

For TPF processing, samples were heated in a custom build TPF apparatus under vacuum to the desired processing temperature (between 703 K and 723 K), at which AMZ4 reaches the highly viscous supercooled liquid (SCL) state. The samples were held isothermally for a defined time while the applied pressure caused viscous flow and plastic deformation. Subsequently, the samples were cooled back into the glassy state with the help of a Peltier element reaching cooling rates in the order of 10 K/s [17,18]. The maximum pressing force of the device is F = 4500 N. Details about the technique and the apparatus as well as a sophisticated study of TPF process parameters for cast AMZ4 samples can be found in previous works [10,18]. In the present study, three setups are tested. An overview of the setups, used sample geometries, and applied analysis methods can be found in Fig. 1.

For setup (A), beam-shaped samples were loaded with a comparably low pressing force of F = 500 N for t = 30 s at a temperature of T = 713 K to test, in principle, the influence of TPF on the thermophysical and mechanical properties. The relatively low force caused only slight deformation of the sample and allows subsequent mechanical testing of the beam.

In setup (B), the possibility to increase the surface quality of as-built LPBF samples was tested. Thereby, cylindrical specimens were placed in a suitable setup consisting of a casing and two pistons, schematically illustrated in Fig. 1, to prevent massive deformation through viscous flow and were loaded to smoothen the rough upskin surface. The process parameters were set to F = 4500 N, t = 40 s, and T = 723 K.

In setup (C), a finely structured hard metal template, provided by Olympus Surgical Technologies Europe, was pressed into a sanded beam sample to demonstrate the possibility to imprint a complex surface pattern, as shown in principle in Fig. 1. In this case the used processing parameters were F = 3000 N, t = 30 s, and T = 703 K.

Mechanical testing of beam-shaped LPBF-formed samples in as-built condition (LPBF-AB) and after TPF post-processing according to setup (A) (LPBF-TPF) was performed in three-point bending (3PB) mode to obtain stress-strain curves using a Shimadzu testing machine, as described in [16]. The surfaces of the beams to be tested were sanded to achieve a well-defined geometry and surface roughness. The amorphous state of LPBF-AB and LPBF-TPF samples was verified by calorimetry and X-ray diffraction. A power compensated Perkin Elmer DSC 8000 was used to perform temperature scan measurements with a constant heating rate of 1 K/s between 373 and 853 K in aluminum pans under argon flow to allow the quantification of the glass transition temperature T_g, the starting temperature of crystallization T_x, and the enthalpy of crystallization ΔH_x. X-ray diffraction was performed in a range of angles (2θ) between 20° and 80° with a PANalytical X'Pert Pro diffractometer using Cu-K_α radiation. Furthermore, high-energy synchrotron X-ray diffraction (HESXRD) of an as-cast reference as well as a LPBF-AB and LPBF-TPF sample was measured at the P21.2 beamline facility of PETRA III of the Deutsche Elektronen-Synchrotron (DESY). Measurements at room temperature were performed with a wavelength of 0.177138 Å (70 keV) in transition mode, using a VAREX XRD4343CT detector (2880 × 2880 pixels). The two dimensional diffraction pattern were integrated using PyFAI and further processed using the PDFgetX2 software to obtain the total structure factor S(Q).

Testing of surface roughness of the upper surface of the cylindrical samples before and after TPF-treatment according to setup (B) was done by a tactile method, using a Mitutoyo SJ-400 device in analogy with the DIN EN ISO 4288 standard. Yet, the dimensions of the sample limited the evaluation length to the sample diameter of 12 mm. Optical microscopy was performed using an Olympus BX51 device. Thereby, the

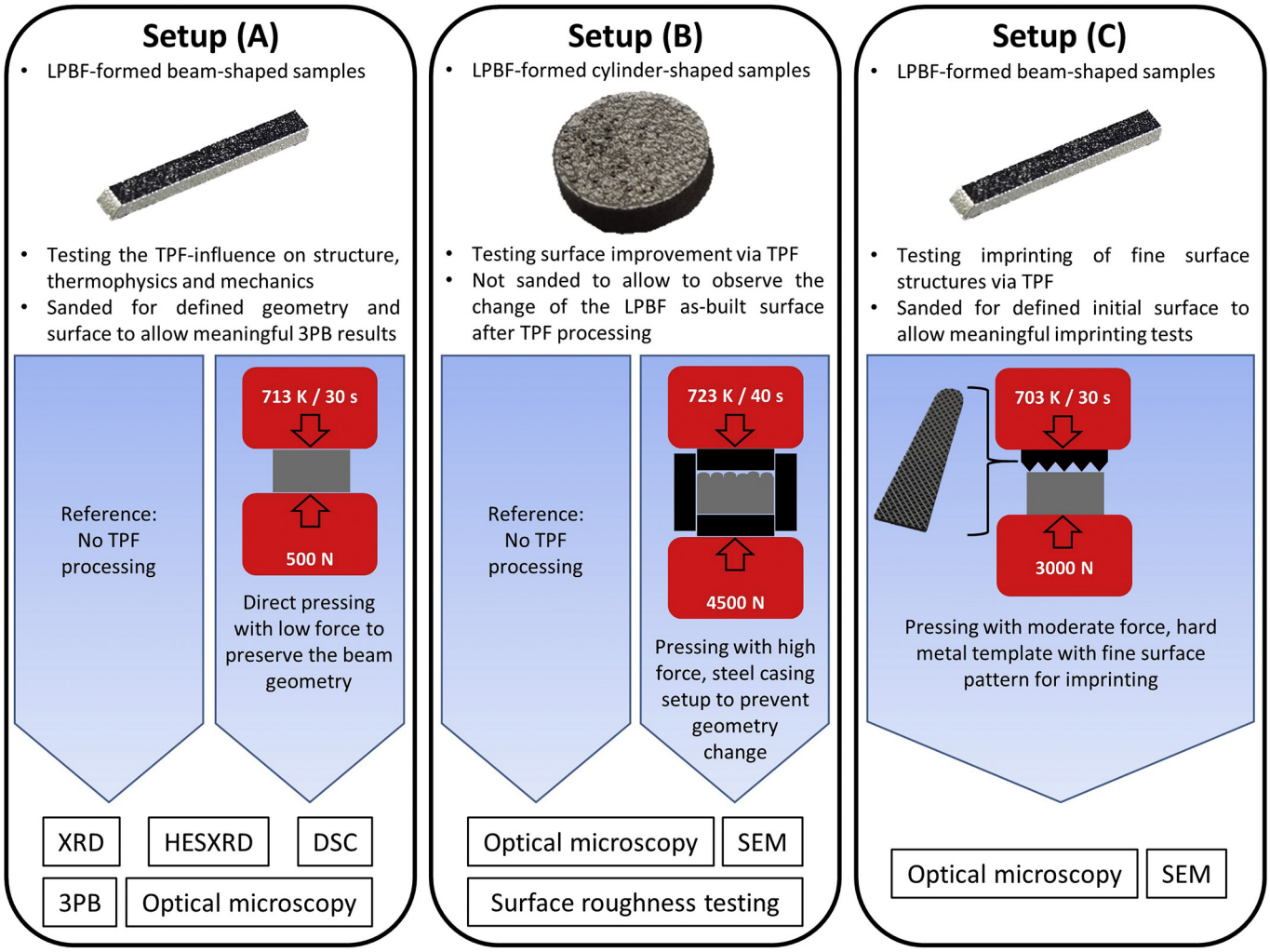

Fig. 1. Overview of the three TPF processing setups, the sample geometries with their respective surface treatment, and the subsequently used analysis methods.

optical density of LPBF-formed beams was determined using the Stream software provided by Olympus GmbH. Scanning electron microscopy was done using a Zeiss Sigma VP device in secondary electron imaging mode.

3. Results

The relative density analysis via optical microscopy reveals that the beam samples before and after TPF setup (A) feature high and basically identical densities of 99.62 ± 0.2% and 99.66 ± 0.2%, respectively. Remaining porosity appears to be mostly spherical gas pores, as can be seen in Fig. A of the Supplementary material.

Fig. 2 compares DSC, XRD, and 3PB results of an as-built LPBF-formed beam (termed LPBF-AB, black curves) and an identical LPBF-formed beam after TPF (termed LPBF-TPF, red curves) according to setup (A). Both diffractograms that are displayed in Fig. 2a do not show Bragg peaks which would reflect a major volume fraction of crystals in the specimens. Instead the diffractograms show a typical broad halo, indicating an overall amorphous structure within the detection limits of this method. In Fig. 2b, both DSC curves show a glass transition from the initial glassy state into the supercooled liquid state at glass transition temperatures T_g of 683 K (LPBF-AB) and 680 K (LPBF-TPF). Crystallization occurs for both samples at $T_x = 758$ K, integration over the respective exothermal events reveals the enthalpies of crystallization ΔH_x that are found to be 4.02 kJ/g-atom (LPBF-AB) and 3.91 kJ/g-atom (LPBF-TPF). The results are relatively similar and reflect a typical ΔH_x value for amorphous AMZ4, further validating the overall amorphous nature of the beams [16]. Differences can be found in the slightly differing shape of the crystallization signal as well as in the sub-T_g behavior of both samples. While the LPBF-AB sample indicates distinct structural relaxation in form of an exothermal signal below T_g, such an effect cannot be observed for the LPBF-TPF sample, revealing different relaxation states. In Fig. 2c, the stress-strain curves of both samples show an almost identical behavior with a Young's modulus of about 81 GPa, a fracture strength σ_f of roughly 2.1 GPa, and no observable plastic deformation. In contrast, an AMZ4 sample cast from high-purity material (the oxygen content of the used Zr is about 13 μg/g [19]) shows pronounced plasticity, combined with a Young's modulus of about 76 GPa and a yield stress σ_y of about 2.1 GPa (gray dotted line, taken from reference [18]).

Fig. 3 shows the HESXRD S(Q) results of a high purity as-cast reference AMZ4 sample, a beam-shaped LPBF-AB sample and a LPBF-TPF sample treated according to setup (A). While the as-cast sample shows no Bragg peaks, the LPBF-AB sample features slight reflexes, indicating the presence of a small amount of crystalline fraction in an overall amorphous structure. The LPBF-TPF sample still shows an overall amorphous structure but with a further increased amount and intensity of crystalline reflexes.

Fig. 4a depicts the casing and pistons used to improve the surface roughness of as-built LPBF-samples according to setup (B). The surfaces of a LPBF-AB and a post-processed LPBF-TPF cylinder are compared in

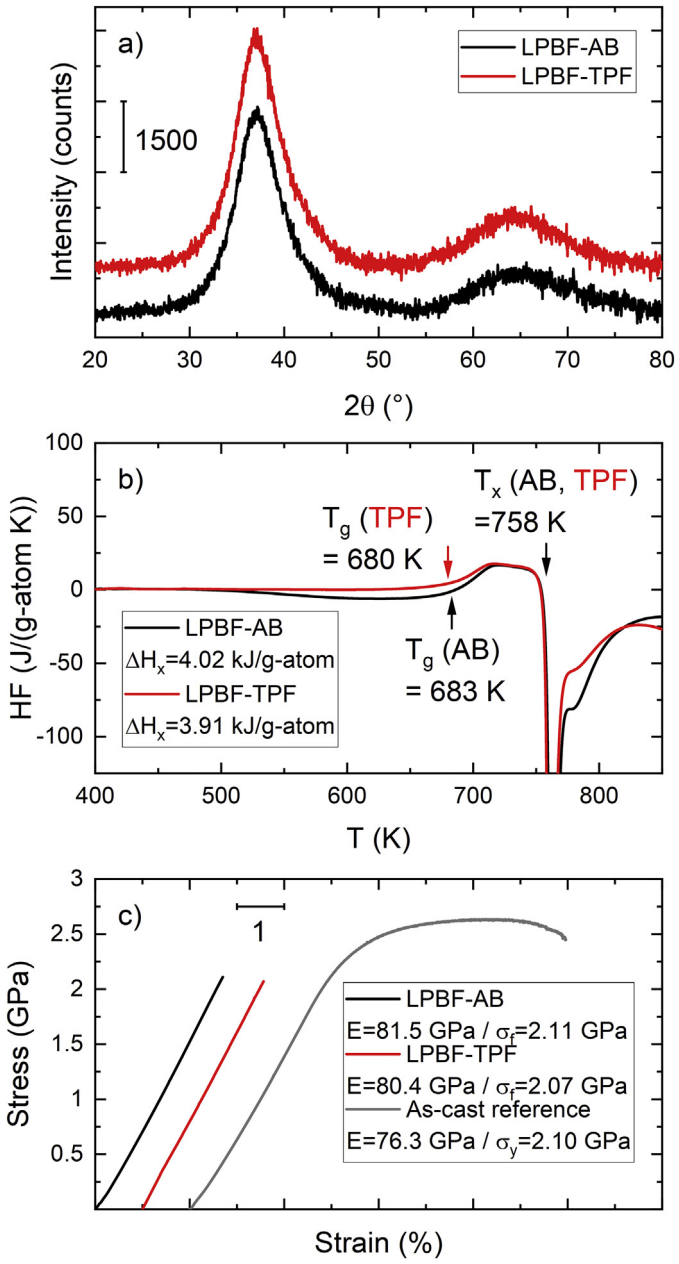

Fig. 2. a) XRD diffractograms of an as-built additionally formed beam-shaped sample (LPBF-AB) and a TPF post-processed (LPBF-TPF) beam, according to setup (A). Both samples show the typical halo, indicating an amorphous structure without crystallites. b) DSC scans of the LPBF-AB and the LPBF-TPF sample. Both of them show a glass transition at about 700 K, followed by the supercooled liquid state and crystallization at roughly 750 K with almost identical crystallization enthalpy ΔH_x. c) Results of the three-point bending mechanical testing. LPBF-AB and LPBF-TPF samples show a similar fracture strength σ_f of about 2.1 GPa without ductile behavior. In contrast, an as-cast reference beam sample reaches its yield strength at 2.1 GPa, followed by remarkable plastic deformation.

Fig. 4b and c. Here, a drastic reduction of surface roughness through the TPF post-processing is visible. This is further quantified by the results of the roughness testing. Without TPF, the R_a and R_z values are 14.2 ± 0.3 μm and 99.4 ± 13.8 μm. After TPF post-processing, these values are reduced by about one order of magnitude to 1.1 ± 0.4 μm and 10.2 ± 3.1 μm, respectively. The TPF-imprinted beam from setup (C) is shown in Fig. 4d, together with the used hard metal template. Due to the lack of containment in contrast to setup (B), bulging through plastic deformation is visible on the side faces of the TPF-pressed part. The surfaces of template and beam are shown in detail in Fig. 4e and with further magnification in the SEM images in Fig. 4f. The overall surface topology of the hard metal template is mirrored on the beam surface. Thereby, even the fine milling cuts of the template are reproduced on the imprinted surface of the BMG part.

4. Discussion

In the present study, the viability to produce amorphous AMZ4 samples using LPBF is confirmed by the XRD and DSC results within the detection limits of these analysis methods. This generally agree with earlier studies published so far [15,16,20–22]. The same applies for the LPBF-TPF sample, demonstrating the applicability of TPF post-processing without major loss of the desired glassy state of the material, if the processing window is judiciously chosen. Mechanical testing reveals that the LPBF-AB and the LPBF-TPF sample are both able to reproduce the yield strength of the high-purity as-cast reference sample. Yet, while the cast sample allows for considerable plastic deformation, the LPBF-formed ones show brittle behavior, causing the yield point and fracture point to coincide. Furthermore, the additively manufactured samples show a slightly higher Young's modulus than the cast reference. Bordeenithikasem et al. [20] reported fracture stresses of about 1.3 GPa for LPBF-formed AMZ4, which is distinctly below the yield strength of the alloy. This effect was i.a. attributed to the presence of irregularly shaped gas pores that act as crack initiation sites and lead to premature sample failure, a commonly observed mechanism in metallic glasses [23–26]. Yet, since very high optical densities above 99.6% with mostly spherically shaped pores are present, as previously reported in [15,16], and since the LPBF-formed AMZ4 in this study shows no premature failure before the yield stress is reached, porosities are not identified as a crucial threat to the mechanical integrity, as previously suggested in reference [16].

Conventional XRD is known to only provide information about the average structure of the investigated sample, thereby leaving small crystalline fractions or especially nano-crystals possibly undetected [27]. At this point, the extremely high flux used for HESXRD helps to detect smaller crystalline fractions, as shown in Fig. 3. The LPBF-AB sample features slight Bragg peaks in the HESXRD S(Q) data, which is in agreement with Pacheco et al., who recently found that small degrees of nano-crystallinity are a common feature of LPBF-formed AMZ4 [22]. Comparing the HESXRD total structure factors of LPBF-AB and the LPBF-TPF sample, the TPF process is found to further increase the degree of crystallinity. This is not surprising as TPF is performed in the supercooled liquid state, where the increased atomic mobility allows crystal nucleation and growth [28]. Based on previous works [29–31], nano-crystalline Zr_4Cu_2O has been identified as the primary crystalline phase that forms during heating of LPBF-formed AMZ4, followed by Al_3Zr_4 and Zr_2Cu [22]. Thus, the same types of nano-crystalline phases can be assumed to be present in a small degree in the LPBF-TPF sample, although the low amount and intensity of the Bragg peaks in Fig. 2 prohibit a clear phase identification. Yet, the increase in crystallinity is still low enough to be concealed by the detection limit of conventional XRD, see Fig. 2a. The change in the DSC crystallization signal shape, see Fig. 2b, and the slightly reduced ΔH_x value seem to reflect the TPF-induced crystallization, yet, it has to be noted that the observed ΔH_x difference of about 0.1 kJ/g-atom is well within the method-typical measurement uncertainty [32–34]. The gradually increased crystallinity of the LPBF-TPF sample seems to be still uncritical in terms of the mechanical properties as no decrease in strength is observed in comparison to the LPBF-AB sample, see Fig. 2c. Schroers et al. recently found that small crystalline fractions in Zr-based BMGs only have marginal influence on the mechanical properties, allowing for robust parts even after TPF processing [28].

In the present work, the absence of ductility can be mainly addressed to intrinsic brittleness of the material due to the high oxygen content, as various studies have demonstrated the increase of brittleness and

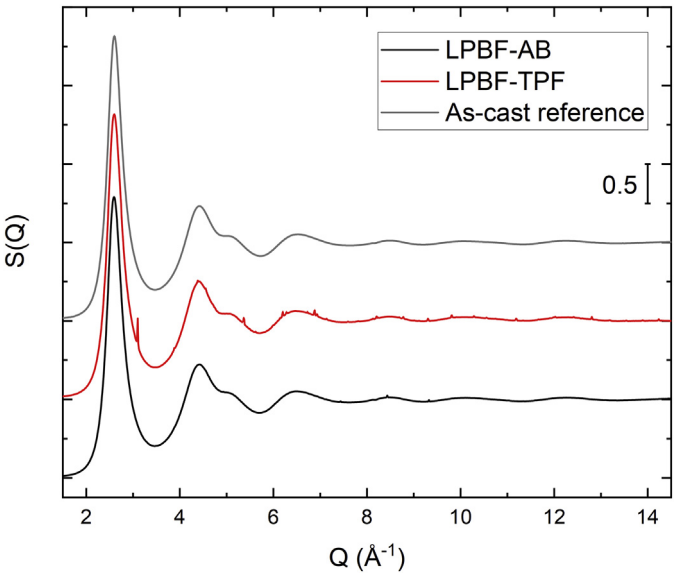

Fig. 3. High-energy synchrotron XRD total structure factors of an as-cast AMZ4 sample, an as-built (LPBF-AB) and a TPF processed (LPBF-TPF) additively formed beam-shaped sample, according to setup (A). The as-cast sample shows a fully amorphous halo without Bragg peaks, while the LPBF-AB sample features three small reflexes, indicating a slight amount of crystalline fraction. The LPBF-TPF sample still shows a mainly amorphous structure, but features an increased amount of Bragg peaks, indicating a higher degree of crystallization in comparison to the as-built sample.

stiffness of Zr-based BMGs through oxygen contamination [35–40]. Oxygen is found to change the short- and medium-range order in the way that shear processes and the formation of multiple shear bands are impeded, thus provoking catastrophic failure [38,40]. The oxygen contamination issue can be traced back to the inherent characteristics of the used powder feedstock, as it features an extremely high surface-to-volume ratio that leads to increased absorption of oxygen during the atomization process [41,42]. Also, oxygen uptake during the LPBF process itself, due to residual oxygen in the build chamber and through residual humidity in the powder feedstock, further contributes to the oxygen contamination [41–43]. Combined, powder atomization and LPBF processing increase the oxygen level massively, up to values of several hundreds or even thousands of μg/g, while Zr-based metallic glasses produced by casting usually feature oxygen levels in the order of only 80 μg/g [42,44]. The obvious difference in terms of ductility between as-cast and LPBF-formed AMZ4 should be interpreted in this context. In principle, TPF processing may lead to a further increase in oxygen contamination. Yet, by taking the rather low processing temperatures in the supercooled liquid state and consequentially sluggish diffusion processes into account, the influence of the TPF process should rather be neglectable. This approach seems valid as the mechanical performance is not harshly altered by TPF at all.

The exothermal structural relaxation signal found for the LPBF-AB sample in Fig. 2b is a typical result of a fast cooling process present during vitrification [45], which is not surprising if taking the process-typical high cooling rates of up to 10^6 K/s into account [6]. In contrast, the LPBF-TPF sample does not feature a significant structural relaxation signal, reflecting the much slower cooling rate of roughly 10 K/s that is achievable with the used device [17,18] and by conductive cooling through the sample volume itself.

Thermoplastic forming has been reported to have a negative influence on the ductility of BMGs since slowly cooled glasses are structurally more relaxed, corresponding to a lower free volume and a lower enthalpic state [45,46], and therefore tend to show increased brittleness [47–49]. Yet, the present findings suggest that the influence of the relaxation state is rather neglectable as the oxygen embrittlement dominates the mechanical behavior, before and after TPF post-processing. So, in case of the present alloy and process conditions, the mechanical properties before and after TPF can be assumed to be identical, thereby simplifying the overall prediction of expectable mechanical performance of a post-processed part. This decoupling of mechanical performance and the TPF process further underlines its applicability as a viable post-processing route.

First tests to increase the surface quality of an LPBF-formed sample in setup (B), see Fig. 4b and c, show promising results by drastically lowering the roughness. Yet, residual artifacts remain visible, most likely caused by initial irregularities in the LPBF-formed surface that were too massive to be smoothed out in the present experimental setup. Here, further testing campaigns for parameter optimization are needed. Pretreating the LPBF surface before starting the TPF process by e.g. grit blasting or sanding could erase protruding irregularities and, thus, increase the surface quality achievable by TPF. The potential of such an approach is shown by the results of setup (C) in Fig. 4e and f. The previously sanded beam precisely reproduces the TPF-imprinted template and demonstrates the generally known net-shape formability of BMGs [48,50] for the first time in case of an additively formed part.

A more complex TPF template form that combines the given part containment from setup (B) with the fine structure pattern of setup (C) could be used to add a functional surface to a LPBF-formed part without changing its overall geometry through undesired plastic deformation. Such a production route would allow to combine the geometrical freedom of additive manufacturing with a tailorable application-oriented surface optimization in part regions where it is explicitly needed. This is of interest especially for components that are too complex to be formed by casting and require surface qualities that are difficult to achieve by machining. Examples can be found in medical applications, e.g. for technology used for minimal-invasive surgeries. Fig. 5 schematically demonstrates such a LPBF-TPF production route for a minimal-invasive clamp device. For this application, both clamp halves have to provide form closure, and therefore demand for a precisely defined surface pattern with low tolerances, which is applied by a local TPF post-treatment.

If only a relatively small area with a defined surface pattern is needed, an even more straight forward approach could be found that renounces the use of a complex containment setup. Thereby, a small heated template piston is to be pressed onto the respective area. The surface is locally heated into the supercooled liquid state and is imprinted by the piston template, while the surrounding volume remains cold and in the undeformed glassy state. After imprinting, the piston template is removed, and the deformed surface area is cooled quickly by the ambient material. Such a localized approach is especially suitable for jewelry applications, where e.g. complexly skeletonized LPBF parts could be surface finished or even personalized (similar to an embossing process) through imprinting. Here, Pt-based BMG systems would be promising candidates, since they combine high thermal stability against crystallization, ductile mechanical behavior even after slow cooling, and a high resistance against oxygen absorption due to the noble metal character [49,51].

Furthermore, a recent study by Bochtler et al. demonstrated the principal possibility to use TPF for consolidation of AMZ4 powder to highly dense bulk material with a low minimal porosity [18]. In the present study, the density measurements suggest that the LPBF-formed samples already show a porosity level low enough to remain unchanged after TPF processing, most likely since closed gas pores embedded in the bulk material cannot easily be erased through pressing in the supercooled liquid state. Yet, the results by Bochtler et al. [18] suggest that TPF could be a valid option to increase the relative density of additively formed BMG-parts with higher degrees of porosity, leaving this approach as a possible topic of future studies. A similar post-processing technique is already established for crystalline additively formed metals in form of hot isostatic pressing (HIP) [52,53].

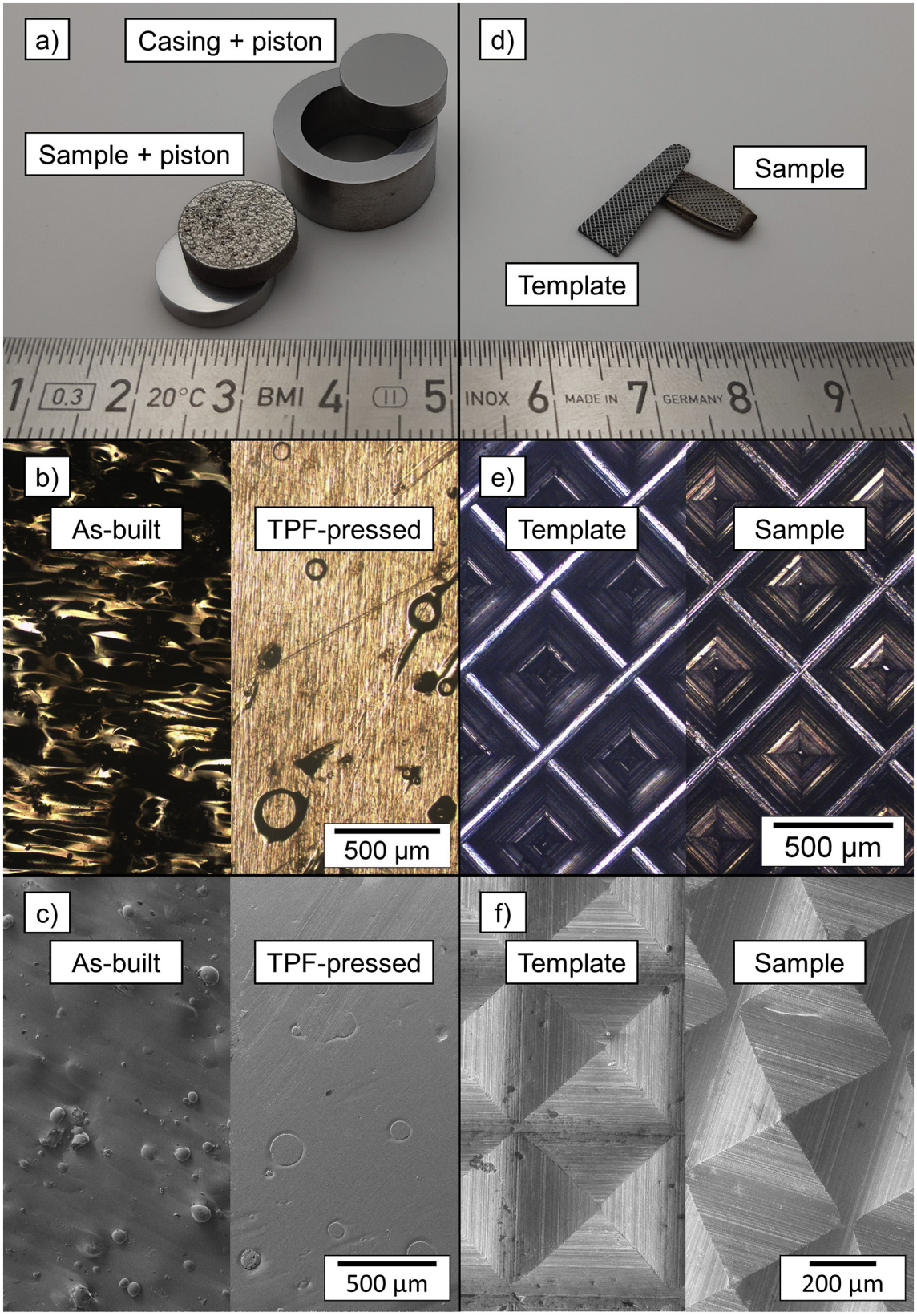

Fig. 4. a) Piston set used for TPF setup (B), consisting of two polished pistons and a cylinder casing, that allows to press and smoothen the rough surface of an LPBF as-built cylinder (placed on top of the lower piston) without severe change of geometry through plastic deformation. Optical microscopy image, b), and SEM secondary electron contrast image, c), of the as-built (left) and TPF-pressed cylinder surfaces in direct comparison. d) Hard metal template (left) and imprinted LPBF-formed beam (right) from setup (C). e) The surface structure of the template shows a periodic structure with fine milling cuts (left), which is directly mirrored on the imprinted beam (right). The respective SEM secondary electron images, f), confirm the remarkable surface reproduction.

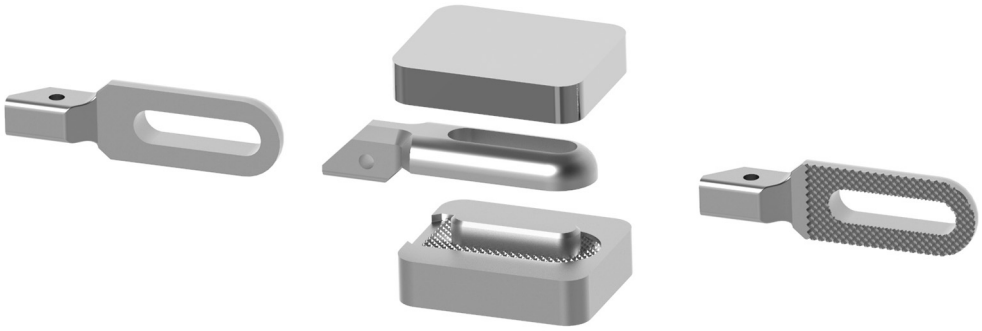

Fig. 5. TPF post-processing can be used to add finely structured surface patterns to additively formed BMG parts in regions that demand special surface requirements. In this schematic example, a LPBF-formed half of a clamp device used for minimal-invasive surgery is locally imprinted with a fine grit pattern using a template that features the negative shape of the desired pattern. Due to local containment around the TPF-processed region, severe geometry change through plastic deformation is avoided.

5. Conclusion

Overall amorphous AMZ4 specimens were produced by LPBF additive manufacturing according to previous studies. The possibility of TPF post-processing of these samples is explored in the present work, leading to three conclusions: 1) In principle, LPBF-formed AMZ4 provides enough thermal stability to withstand TPF without severe crystallization effects. Synchrotron XRD may allow to detect small degrees of crystallinity induced by TPF, but the mechanical properties remain mostly unchanged on a high level and encourage industrial applications. 2) The typical surface roughness of as-built LPBF-formed samples can be drastically reduced through TPF, albeit preliminary steps like sanding or sand blasting might be needed to get completely rid of remaining surface artifacts. 3) Imprinting of sanded LPBF-formed AMZ4 can create TPF-typical near-perfect surface pattern.

Due to their unique amorphous structure, BMGs are the only metallic materials that offer the possibility to apply thermoplastic forming. The present study provides the proof of principle that this net-shape creating method can be used to post-process additively formed metallic glasses. This is a distinct advantage over additively formed crystalline alloys and allows for novel production routes, especially for medical and jewelry applications.

Data availability

The raw/processed data required to reproduce these findings cannot be shared at this time as the data also forms part of an ongoing study.

Declaration of Competing Interest

The authors declare that they have no known competing financial interests or personal relationships that could have appeared to influence the work reported in this paper.

Acknowledgements

The authors want to thank Moritz Stolpe from Heraeus Amloy Technologies GmbH for providing powder material. We further acknowledge DESY (Hamburg, Germany), a member of the Helmholtz Association HGF, for the provision of experimental facilities. Parts of this research were carried out at PETRA III and we would like to thank Malte Blankenburg and Ulrich Lienert for assistance in using the P21.2 beamline facility. This research was funded by the German Federal Ministry for Economic Affairs and Energy (BMWi) within the Promotion of Joint Industrial Research Programme (IGF) due to a decision of the German Bundestag. It was part of the research projects 19927N (OptMetGlas) and 21227N (LaSaM) by the Association for Research in Precision Mechanics, Optics and Medical Technology (F.O.M.) under the auspices of the German Federation of Industrial Research Associations (AiF).

Appendix A. Supplementary data

Supplementary data to this article can be found online at https://doi.org/10.1016/j.matdes.2020.109368.

References

[1] M. Telford, Materialstoday 7 (2004) 36–43.
[2] S. Pauly, L. Löber, R. Petters, M. Stoica, S. Scudino, U. Kühn, J. Eckert, Mater. Today 16 (2013) 37–41.
[3] X.P. Li, M.P. Roberts, S. O'Keeffe, T.B. Sercombe, Mater. Des. 112 (2016) 217–226.
[4] Z. Mahbooba, L. Thorsson, M. Unosson, P. Skoglund, H. West, T. Horn, C. Rock, E. Vogli, O. Harrysson, Appl. Mater. Today 11 (2018) 264–269.
[5] E. Williams, N. Lavery, J. Mater. Process. Technol. 247 (2017) 73–91.
[6] P.A. Hooper, Addit. Manuf. 22 (2018) 548–559.
[7] M. Lowther, S. Louth, A. Davey, A. Hussain, P. Ginestra, L. Carter, N. Eisenstein, L. Grover, S. Cox, Addit. Manuf. 28 (2019) 565–584.
[8] V. Urlea, V. Brailovski, J. Mater. Process. Technol. 242 (2017) 1–11.
[9] N. Mohammadian, S. Turenne, V. Brailovski, J. Mater. Process. Technol. 252 (2018) 728–738.
[10] B. Bochtler, O. Kruse, R. Busch, J. Phys. Condens. Matter 32 (2020) 1–11.
[11] Y. Saotome, Y. Fukuda, I. Yamaguchi, A. Inoue, J. Alloys Compd. 434–435 (2007) 97–101.
[12] G. Kumar, A. Desai, J. Schroers, Adv. Mater. 23 (2011) 461–476.
[13] K. Kosiba, L. Deng, S. Scudino, Materials (Basel) 13 (2020).
[14] J. Heinrich, R. Busch, B. Nonnenmacher, Intermetallics 25 (2012) 1–4.
[15] J. Wegner, S. Kleszczynski, M. Frey, S. Hechler, G. Witt, R. Busch, Proc. 15th Rapid. Tech Conf, 2018.
[16] J. Wegner, M. Frey, P. Stiglmair, S. Kleszczynski, G. Witt, R. Busch, South African J. Ind. Eng. 30 (3) (2019) 32–40.
[17] M. Kelkel, Master Thesis (2016) 111.
[18] B. Bochtler, M. Stolpe, B. Reiplinger, R. Busch, Mater. Des. 140 (2018) 188–195.
[19] J. Heinrich, Massivglasbildende Metallische Legierungen Als Konstruktionswerkstoff Materialoptimierung Und Technologieentwicklung Zur Herstellung Und Verarbeitung, 2012.
[20] P. Bordeenithikasem, M. Stolpe, A. Elsen, D.C. Hofmann, Addit. Manuf. 21 (2018) 312–317.
[21] J.J. Marattukalam, V. Pacheco, D. Karlsson, L. Riekehr, J. Lindwall, F. Forsberg, U. Jansson, M. Sahlberg, B. Hjörvarsson, Addit. Manuf. 13 (2020) 101124.
[22] V. Pacheco, D. Karlsson, J.J. Marattukalam, M. Stolpe, B. Hjörvarsson, U. Jansson, M. Sahlberg, J. Alloys Compd. 825 (2020).
[23] C.J. Lee, Y.H. Lai, J.C. Huang, X.H. Du, L. Wang, T.G. Nieh, Scr. Mater. 63 (2010) 105–108.
[24] J. Zhang, D. Estévez, Y.Y. Zhao, L. Huo, C. Chang, X. Wang, R.W. Li, J. Mater. Sci. Technol. 32 (2016) 129–133.
[25] A. Kuball, B. Bochtler, O. Gross, V. Pacheco, M. Stolpe, S. Hechler, R. Busch, Acta Mater. 158 (2018) 13–22.
[26] A.S. Nouri, X.J. Gu, S.J. Poon, G.J. Shiflet, J.J. Lewandowski, Philos. Mag. Lett. 88 (2008) 853–861.
[27] C. Suryanarayana, A. Inoue, Bulk Metallic Glasses, CRC Press, 2011.
[28] J. Ketkaew, Z. Liu, W. Chen, J. Schroers, Phys. Rev. Lett. 115 (2015) 1–6.
[29] J. Eckert, N. Mattern, M. Zinkevitch, M. Seidel, Mater. Trans. JIM 39 (1998) 623–632.
[30] M.F. De Oliveira, W.J. Botta, M.J. Kaufman, C.S. Kiminami, J. Non. Cryst. Solids 304 (2002) 51–55.
[31] M.F. de Oliveira, M.J. Kaufman, W.J. Botta Filho, C.S. Kiminami, Mater. Sci. Forum 386–388 (2002) 53–58.

[32] N. Neuber, O. Gross, M. Eisenbart, A. Heiss, U.E. Klotz, J.P. Best, M.N. Polyakov, J. Michler, R. Busch, I. Gallino, Acta Mater. 165 (2018) 315–326.
[33] M. Frey, R. Busch, W. Possart, I. Gallino, Acta Mater. 155 (2018) 117–127.
[34] O. Gross, B. Bochtler, M. Stolpe, S. Hechler, W. Hembree, R. Busch, I. Gallino, Acta Mater. 132 (2017) 118–127.
[35] V. Keryvin, C. Bernard, J.C. Sanglebœuf, Y. Yokoyama, T. Rouxel, J. Non, Cryst. Solids 352 (2006) 2863–2868.
[36] Y. Yokoyama, A. Kobayashi, K. Fukaura, A. Inoue, Mater. Trans. 43 (2002) 571–574.
[37] X.H. Lin, W.L. Johnson, W.K. Rhim, Mater. Trans. JIM 38 (1997) 473–477.
[38] Z.P. Lu, H. Bei, Y. Wu, G.L. Chen, E.P. George, C.T. Liu, Appl. Phys. Lett. 92 (2008) 1–4.
[39] J.P. Best, H.E. Ostergaard, B. Li, M. Stolpe, F. Yang, K. Nomoto, M.T. Hasib, O. Muránsky, R. Busch, X. Li, J.J. Kruzic, Addit. Manuf. (2020) 101416.
[40] J.P. Best, J. Ast, B. Li, M. Stolpe, R. Busch, F. Yang, X. Li, J. Michler, J.J. Kruzic, Mater. Sci. Eng. A 770 (2020) 138535.
[41] J.H. Tan, W.L.E. Wong, K.W. Dalgarno, Addit. Manuf. 18 (2017) 228–255.
[42] L. Deng, K. Kosiba, R. Limbach, L. Wondraczek, U. Kühn, S. Pauly, J. Mater. Sci. Technol. 60 (2021) 139–146.
[43] K. Dietrich, J. Diller, S. Dubiez-Le Goff, D. Bauer, P. Forêt, G. Witt, Addit. Manuf. 32 (2020).
[44] S. Pauly, C. Schricker, S. Scudino, L. Deng, U. Kühn, Mater. Des. 135 (2017) 133–141.
[45] Z. Evenson, I. Gallino, R. Busch, J. Appl. Phys. 123 (2010) 529.
[46] A. van den Beukel, J. Sietsma, Acta Metall. Mater. 38 (1990) 383–389.
[47] G. Kumar, D. Rector, R.D. Conner, J. Schroers, Acta Mater. 57 (2009) 3572–3583.
[48] J. Schroers, Adv. Mater. 22 (2010) 1566–1597.
[49] G. Kumar, P. Neibecker, Y.H. Liu, J. Schroers, Nat. Commun. 4 (2013) 1536.
[50] J. Schroers, J. Miner. Met. Mater. (2005) 35–39.
[51] O. Gross, S.S. Riegler, M. Stolpe, B. Bochtler, A. Kuball, S. Hechler, R. Busch, I. Gallino, Acta Mater. 141 (2017) 109–119.
[52] C.B. Finfrock, A. Exil, J.D. Carroll, L. Deibler, Metallogr. Microstruct. Anal. 7 (2018) 443–456.
[53] W. Tillmann, C. Schaak, J. Nellesen, M. Schaper, M.E. Aydinöz, K.P. Hoyer, Addit. Manuf. 13 (2017) 93–102.